Charge Transfer through a Protein−Nano Junction

Nadine Utz and Thorsten Koslowski*

Institut für Physikalische Chemie, Universität Freiburg, Albertstrasse 23a, D-79104 Freiburg im Breisgau, Germany

Received: December 12, 2005; In Final Form: March 16, 2006

We address the problem of charge transfer (CT) between a nanosized inorganic system and a protein from a theoretical and numerical perspective. The CT process is described on an atomistic level by applying an electronic Hamiltonian that takes into account the chemical bond, vibronic coupling effects, and polarization degrees of freedom. As a structurally well-characterized example, we consider a complex of C_{60} and its antibody. For this system, we find a novel efficient protein CT mechanism; through-space superexchange is mediated by stacked π orbital systems. The predicted rates are comparable to those obtained for short-range electron tunneling through covalent bonds, the fastest ground-state CT process known for proteins.

1. Motivation and Introduction

Functional biochemical aggregates and man-made nanosystems exist on the same length scale and exhibit a wide spectrum of interactions. It has become one of the motivations of chemistry and physics at the bio−nano interface to understand their interplay to tailor nanoparticles suited for specific applications. Potential utilizations include drug[1,2] and gene[3] delivery systems, carriers for radioactive markers,[4] and templates for the design of pharmaceutical agents.[5,6] In addition, sensing and analyzing single biomolecules will play an increasing role in the future. The corresponding nanotechnology-based biosensors have to fulfill two requirements: a high specifity and a means to rapidly transfer information from the nanoscale level to that of a human observer. The latter can be achieved by amplifying a current generated within the recognition process,[7] with charge transfer (CT) as the underlying molecular mechanism. Bio−nano CT also plays an important role in attempts to combine transiently created charge carriers in biosystems—as electron holes in DNA—and nanoscopic conducting objects such as carbon nanotubes into operative circuits.[8]

Understanding CT between biological and man-made nanostructures at an atomic, nonphenomenological level requires a detailed knowledge of the underlying microscopic structure. As noncovalent links between nano-objects and the molecules of life frequently lack the high specifity of protein−protein interactions, high-resolution structural information regarding bio−nano contacts is sparse. A notable exception has been reported by Erlanger and co-workers, who have not only been able to generate an antibody to a (modified) C_{60} immunogene and measure its immunological response[9] but also to resolve its microscopic geometry by means of an X-ray structure analysis on the 2.25 Å level.[10] Although the crystallized antibody fragment does not contain the fullerene, there is strong evidence for the location of the binding pocket. This has been substantiated by molecular modeling[10] and a large-scale molecular dynamics simulation of a relevant subset of the protein containing a C_{60} molecule.[11] According to these computations, the fullerene is embedded in a shell of aromatic amino acids that supplies multiple π-stacking interactions to selectively bind the antigene.

As C_{60} and its relatives frequently participate in electron-transfer reactions,[15] we will use the C_{60}−antibody complex as a model system for bio−nano CT. Arbitrarily referring to the fullerene as the acceptor, we introduce a mixed valence ruthenium complex covalently bonded to a His residue as a donor, a procedure that is well established in experimental studies of protein charge transfer.[16,17] We thus consider the reaction Ru^{2+}−bridge−$C_{60} \rightleftharpoons Ru^{3+}$−bridge−$C_{60}^{-}$. In the next section we describe the underlying structural model and the techniques that enable the computation of ground-state charge-transfer rates. Numerical results will be presented and discussed in the third section, and conclusions are derived in the final part of the paper.

2. Model and Methods

As a geometric basis of the molecular dynamics simulations, the X-ray structure of an anti-Buckminsterfullerene antibody F_{ab} fragment was used (PDB code 1EMT).[10] The protein consists of a light (L) and a heavy (H) chain; the C_{60} molecule was docked at the suggested binding site. The simulation geometries were kindly made available by Ma, Kong, and Noon.[11] Models of the fragment including the C_{60} fullerene have been published by Braden and co-workers[10] and by Noon et al.[11] We will therefore only give a brief outline of the methodology of the latter here. Due to the size of the complex, only atoms located in a sphere of a 16 Å radius around the binding site have been considered within the simulation.[12] This strategy is usually considered as effective even for large substrates binding to proteins, such as ATP[13] ($R_G = 5.2$ Å) or EHD[14] ($R_G = 5.5$ Å), where the values in brackets refer to modeled radii of gyration, which are considerably larger than that of fullerene ($R_G = 3.5$ Å), exhibit a more complex structure, and interact with the protein via much more specific, longer-ranged interactions. The geometrical setup contains 166 water molecules located at the hydrophilic side of the protein, and a fullerene docked into the assumed binding site by inspection. As the original antigene contains a hydrophilic anchor and thus enforces binding near the surface of the protein, only a single large pocket qualifies here. Unlike complex biological substrates, the interactions

* Author to whom correspondence should be addressed. E-mail: Thorsten.Koslowski@physchem.uni-freiburg.de.

10.1021/jp057244w CCC: $33.50
Published on Web 04/18/2006

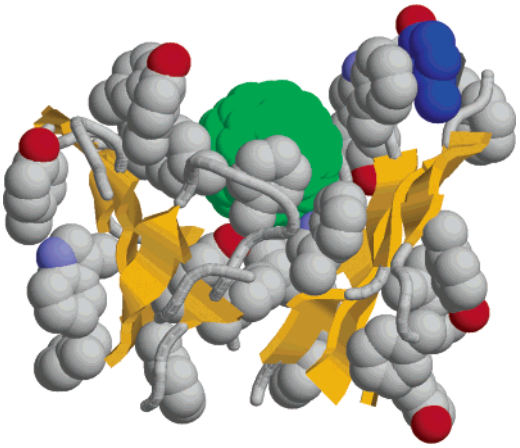

Figure 1. Cartoon model of the binding site of fullerene to its antibody. Snapshot from a molecular dynamics of Noon et al.[11] based upon an X-ray structure of Braden and co-workers.[10] Aromatic amino acid side chains and C_{60} atoms are shown as solid spheres, β-sheets are drawn in yellow, Tyr52H carbon atoms in blue, and C_{60} atoms in green.

between fullerene and its environment completely lack an ionic component, and naturally no hydrogen bonds are formed. Therefore, the docking process itself is not a demanding one. Prior to the molecular dynamics simulations, the structure was minimized and then propagated for a total of 5 ns. As input geometries for the electronic structure computations described below, we have used 10 snapshots from the molecular dynamics (MD) trajectories taken each 500 ps. All further relevant technical details of the simulation are presented in ref 11; a typical snapshot is shown in Figure 1. As Supporting Information of ref 11, a movie illustrating the molecular dynamics trajectory is available.

In the region of interest, the protein does not contain any coordinating site for a ruthenium complex. We have therefore performed a hypothetical Tyr52His one-base mutation in the genetic code, replacing the Tyr52 amino acid in the next-nearest-neighbor coordination shell of the fullerene by a histidine. Both amino acids contain an aromatic side chain; thus the π-stacking interactions around the fullerene remain intact. Both residues are slightly hydrophilic, so a replacement of Tyr at the protein surface should lead to a similar interaction with the solvent. His E2 nitrogens can be coordinated by ruthenium complexes;[16] here we use the $Ru[NH_3]_5^{2+/3+}$ fragment as one of the simplest possible structures. With the His located at the protein surface, the steric requirements for accommodating a moderately sized complex are small (cf. Figure 1). We have checked this conjecture by constructing a model using standard bond lengths without performing an additional geometry optimization.

Charge-transfer reactions are usually described within Marcus' seminal theory[18−20] and its extensions by Sutin, Hush, Dogonadze, Jortner, and many more.[21,22] Charge transfer occurs between a charge donor and a corresponding acceptor, which interact either directly or via a bridge connecting these entities; the latter situation is referred to as electronic superexchange.[23] Donor and acceptor states represent local minima on a free energy surface, and an activation barrier E_A has to be overcome to induce a charge shift. The activation energy, the reorganization energy λ, the so-called driving force ΔG, and the effective tunnel splitting t are required as the input parameters to the computation of the CT reaction coefficients.

A variety of approaches exist to provide a theoretical estimate of these parameters from a microscopic perspective. Generally, the electronic tunnel splitting t lies in the focus of the computations. To our knowledge, calculations of t for proteins have been pioneered by Kuki and Wolynes using a path integral approach.[24,25] With the help of this technique, tunneling paths in proteins can be identified and visualized. More recently, Marcus and co-workers have presented ingenious algorithms such as the preselection of relevant paths[26−28] and sparse matrix methods[29] to enable computations of t for large systems. These calculations permit the treatment of the protein beyond the highly simplified effective medium approach of a two-site donor−acceptor model. Due to the large size of the proteins, empirical one-electron methods such as the extended Hückel theory or simple tight-binding Hamiltonians are applied. The diagonalization of the resulting large Hamiltonian matrices can be avoided by using Green's functions methods.[29] These methods do, however, require the separation of the system into a donor, an acceptor, and a bridge region. This feature is shared with the application of Löwdin's diagonalization method to CT problems.[30] More recent theoretical developments in the field of protein charge transfer have been described[31] as focusing on multipathway approaches, volumetric effects, and the explicit computation of tunneling currents.[32−34] Derived from a quantum mechanical Green's function background, Beratan, Onuchic, Gray, and co-workers have designed the widely used phenomenological *pathways* concept,[35−40] where tunneling probabilities between different amino acids depend on their distance and on the type of interaction, viz. covalent, van der Waals, or mediated by hydrogen bonds. Entire amino acids serve as the smallest unit considered within this approach. Whereas computer simulations of large biochemical systems usually rely on classical force fields, the very substrate of the CT process—an excess electron or hole—requires a quantum mechanical approach. Due to the sheer size of the system, we apply an empirical Hamiltonian, as put forward in a variety of contexts,[41,42] including CT in DNA[43−46] and proteins.[47] The model accounts for the omnipresent chemical bond and suggests a microscopic interpretation of the two contributions to the CT reorganization energy, which can be attributed either to polarization degrees of freedom (outer-sphere reorganization energy) or to vibronic coupling (inner-sphere reorganization energy).[18,19] Full technical details of the model, its limitations, and its parametrization are described in ref 47, and we will only present a broad overview of the method here, accompanied by a pictorial representation.

The chemical bond is described by a simple tight-binding Hamiltonian akin to extended Hückel theory

$$\hat{H}_{TB} = \sum_{ia} \epsilon_{ia} n_{ia} + \sum_{iajb} t_{iajb} c_{ia}^{\dagger} c_{jb} \qquad (1)$$

Here, $c_{ia}^{\dagger}$ and c_{ia} are creation and annihilation operators acting upon a localized basis of hydrogen-like valence atomic orbitals i located at atoms a; n_{ia} is the corresponding number operator. Usually defined between chemically bonded nearest neighbors, we have introduced additional long-range interactions between π systems and carefully parametrized the Hamiltonian on the basis of ab initio density functional computations.[48] For the C_{60} acceptor, we only use 2p functions that are constructed perpendicular to the surface. By a local rehybridization, only a single Ru d orbital binding to the His π system is required on the donor.[47] Full details of the parametrization of the one-electron Hamiltonian are given in the appendix of ref 47, so we will only give a brief outline here. As the basis of the diagonal tight-binding parameters, we take the negative valence orbital ionization potentials, as listed in ref 49. For the dependence of the nearest-neighbor tight-binding matrix upon the bond lengths, we use the parameters of Harrison.[49] Neighbors are defined using the standard Pauling covalent and ionic radii,

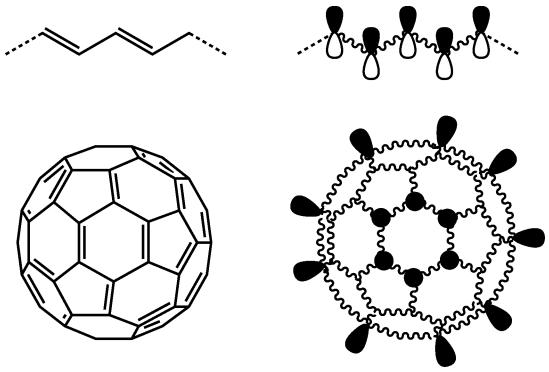

Figure 2. Lewis formulas of polyacetylene (top left) and the C_{60} fullerene (bottom left); a cartoon-style representation of the Su−Schrieffer−Heeger model for these compounds (right). For C_{60}, only some representative p_z-like functions are drawn for convenience.

and orientational effects are taken into account via the familiar Slater−Koster rules.[50] Whereas this parametrization permits a semiquantitative description of the overall electronic structure of biopolymers, we have performed a reparametrization to ensure a more accurate representation of the frontier molecular orbitals, i.e., those parts of the electronic structure that accommodate an excess charge. As a reference, we have used ab initio density functional theory (DFT) calculations of all aromatic amino acids and compounds representing the peptide bond. Finally, long-range interactions between π systems are described by exponentially decaying σ and π coupling matrix elements between $2p_z$-like orbitals. All resulting parameters are listed in ref 47.

In those parts of the system where a naive classification of bonds as single or double does not hold, vibronic coupling has to be taken into account. In the complex studied here, this holds for the fullerene, which exhibits strong bond length and bond order alternation. Vibronic coupling in π systems can be described by the Su−Schrieffer−Heeger (SSH) Hamiltonian[51] via harmonic forces—which are represented as springs in Figure 2—and a distance-dependent matrix element that couples two adjacent $2p_z$ carbon atomic orbitals. This dependence upon distance is linearized in the vicinity of a typical carbon−carbon bond length. For reasons that will become apparent below, it is favorable to work with the bond order rather than the bond length. Chemical intuition suggests an intimate relation between these two quantities, which can be calculated as linear within the SSH model.[52] Within the restricted Hartree−Fock (HF) mean-field approximation, the transformed electron−phonon coupling part of the Hamiltonian is given by[52]

$$\hat{H}_{\mathrm{SSH}} = -4U_{\mathrm{SSH}} \sum_{\langle ab \rangle} [\bar{n}_{ab}(c_a^{\dagger}c_b + c_b^{\dagger}c_a) - \bar{n}_{ab}{}^2] \qquad (2)$$

where the $\bar{n}_{ab}$ are the tight-binding bond orders. We define the so-called off-diagonal Hubbard parameter $U_{\mathrm{SSH}} = \alpha^2/2k$, which is equal to 0.32 eV for nearest neighbors—as indicated by the angular brackets—in the standard SSH model. Here, k denotes the harmonic force constant, and α is the electron−phonon coupling constant.

The outer-sphere reorganization terms are approximated by a nonretarded reaction field. We write the reorganization energy λ_{out} emerging from an ensemble of excess charges Δz_a localized within spheres of radii σ_a in a polarizable environment with a static dielectric constant ϵ_s as[18,19]

$$\lambda_{\mathrm{out}} = \frac{e^2}{4\pi\epsilon_0}\left(\frac{1}{\epsilon_\infty} - \frac{1}{\epsilon_s}\right)\left(\sum_a \frac{\Delta z_a{}^2}{\sigma_a} - \sum_{a<b} \frac{\Delta z_a \Delta z_b}{r_{ab}}\right) \qquad (3)$$

For a single ion, the underlying physical chemistry is illustrated in Figure 3. Neglecting the long-range Coulomb interactions, as also done in the tight-binding part of the Hamiltonian, replacing the charges Δz_a by the corresponding number operators n_a, and applying the Hartree−Fock mean-field expression, we arrive at[41]

$$\hat{H}_{ee} = -\sum_a U[2n_a(\bar{n}_a - \bar{n}_{a,0}) - \bar{n}_a{}^2 + \bar{n}_{a,0}{}^2] \qquad (4)$$

From a slightly different angle, we may consider C_{60} as a sphere carrying a *surface* charge Δz, which is again embedded in a polarizable medium. This approach leads to an identical solution of Poisson's equation for a single sphere of diameter σ_s as for a charge located in the center of sphere, as also suggested by elementary symmetry arguments. Similar to the noninteracting terms of eq 3, its potential energy reads

$$V = \frac{e^2}{4\pi\epsilon_0}\left(\frac{1}{\epsilon_\infty} - \frac{1}{\epsilon_s}\right)\frac{\Delta z^2}{\sigma_s} \qquad (5)$$

We may now break up this effective interaction into contributions stemming from the individual carbon atoms and neglect the interatomic effective Coulombic self-interactions—which are likely to be well-screened on the C_{60} surface—via $\Delta z^2 \simeq \sum_a \Delta z_a^2$ and arrive at an expression that exhibits the same dependence on the atomic excess charges Δz_a as the noninteracting part of eq 3. It can again be treated using the mean-field expression, eq 4, referenced above.

The combined eqs 2 and 4 constitute the mean-field approach to a *model Hamiltonian*. It is meant to capture the essential physical characteristics of charge transfer in a large and complex system, a problem not yet within the reach of more sophisticated quantum chemical approaches. The negative signs of the U and the U_{SSH} parameters indicate that within this model the net electron−electron interaction becomes effectively attractive. Naturally, within the underlying microphysical theories of matter electronic charges are mutually repulsive. Coupling to a solvent or to vibrational degrees of freedom does, however, favor a local accumulation of charges, a situation familiar in condensed matter physics with Cooper pairing—as described within the BCS theory of superconductivity—as the most prominent textbook example. In the terminology of theoretical solid-state physics, eq 4 is referred to as the interaction term of a spin-free attractive Hubbard Hamiltonian.[53,54] Due to their character as centers of excess charge localization, only the transition metal ion and the C_{60} carbon atom attractive Hubbard parameters are set to a nonzero value. Here, $U = 0.8$ eV has turned out to be a parameter adequately representing both transition metal ions[47] and π orbital systems.[43,59]

The combined contributions to the electronic structure—chemical bond (eq 1), vibronic coupling (eq 2), and polarization (eq 4)—can be efficiently solved using an iterative self-consistent field procedure.[52] We obtain potential energy surfaces as a function of the charges $\bar{n}_a$ and bond orders $\bar{n}_{ab}$ as displayed in the following section, which can in turn be analyzed to compute the energy parameters relevant to Marcus' theory of charge transfer.[18,19] These are the reorganization energy λ as the vertical optical transition at the self-consistent field (SCF) minimum, the effective electronic tunnel splitting $2t$ as the highest occupied molecular orbital (HOMO)−lowest unoccupied molecular or-

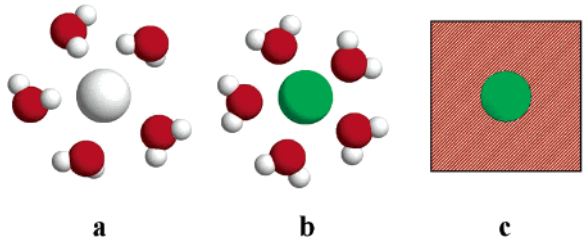

Figure 3. Solvent polarization, as treated within the simplest version of Marcus' theory. (a) Neutral atom coordinated by a shell of water molecules. (b) Charged ion of the same size and reoriented solvation shell. (c) Representation of the system by a charged hard sphere and a dielectric continuum. Parts a and b do not emerge from computations or simulations but are only drawn as cartoons illustrating the underlying physical chemistry.

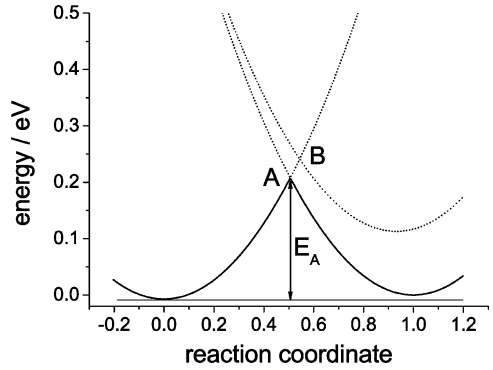

Figure 4. Linear synchronous transit potential energy surface for charge transfer from ruthenium to C_{60}; low-energy CT path (A) and two high-energy CT paths (B).

bital (LUMO) separation at the saddle point and the so-called driving force of the reaction, ΔG. As an alternative, one may consider t and the left and right activation barriers E_A. For a vanishing ΔG and at small t, the reaction rate can be estimated as[18,19]

$$k_{CT} = \frac{t^2}{\hbar}\sqrt{\frac{\pi}{\lambda k_B T}}\exp\left(-\frac{E_A}{k_B T}\right) \qquad (6)$$

3. Results

For each of the 10 MD snapshots, we obtain two ground-state minima resulting from the HF-SCF electronic structure computation, one mainly corresponding to localization of the excess charge on a ruthenium d orbital, the other to a charge delocalized over the fullerene. Between the charge distributions characterizing each of these minima, we may linearily interpolate between the associated density matrices; the interpolation parameter also serves as a convenient reaction coordinate. This procedure is intimately related to the linear synchronous transit approach used by Clark et al. to describe inner-sphere CT reactions between small molecules[55] and the adiabatic charging strategy advocated by Warshel[56] and Chandler and co-workers.[57] A typical cross-section of the potential energy surface thus obtained is shown in Figure 4. It resembles the familiar picture of intersecting parabola with the peculiarity of three low-lying acceptor levels, which originate from the three LUMOs of the C_{60} fragment. At the avoided crossings, we directly obtain the effective electronic couplings $2t$ as the splitting between the participating donor and acceptor states. As the crossing from a donor to an acceptor level is a rare event for the couplings encountered here, we may safely regard the three CT channels as kinetically independent. Consequently, the reaction coefficients for each process can be summed to give an effective

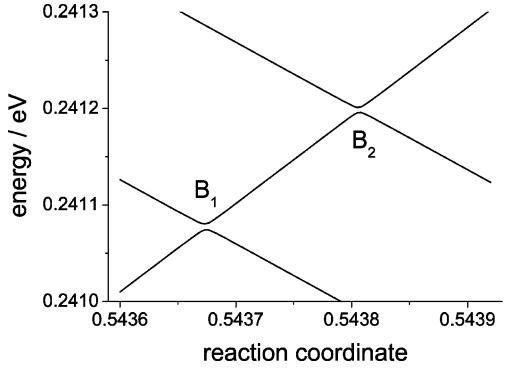

Figure 5. Closeup of Figure 4 in the region of the saddle points of the high-energy charge-transfer paths.

overall k_{CT}, which constitutes the observable total CT rate. We note that a high numerical resolution and particular care are required for resolving the relatively small couplings encountered here (cf. Figure 5), which limits the number of realizations to be considered in the computation of k_{CT}. The extended SSH model Hamiltonian is not sensitive to many-body or correlation effects, as probed on the level of complete random phase approximation (RPA) and Tamm−Dancoff approximation (TDA) calculations, which we have performed for smaller test systems at the stationary points of the potential energy surface, i.e., the minima and the saddle point. We attribute this behavior to the purely attractive, spin-independent character of the electron−electron interaction as used within the polarizable SSH model Hamiltonian applied here.

The resulting effective tunnel splittings amount to $\log_{10} t = -5.5 \pm 0.7$ eV for the low-energy CT path and $\log_{10} t = -5.5 \pm 0.5$ eV for the two high-energy paths. Hence, t does not depend on the CT path, and the two results can be combined to obtain an average based upon 30 t values. With biopolymers showing a high degree of structural flexibility at room temperature, it comes as no surprise that the t values exhibit strong fluctuations. This behavior also has been observed in simulation approaches to charge transfer within proteins and DNA oligomers,[46] where the effective couplings t and the reaction coefficients k_{CT} exhibit exponential distributions. The activation barriers for the forward reaction amount to 215 ± 1 and 248 ± 1 meV for the high- and the low-energy path, respectively. From these values and $\lambda \simeq 950$ meV, a total room-temperature reaction rate of $k_{CT} = 60\ s^{-1}$ emerges. Approaching the inverse regime of CT by tuning ΔG until E_A vanishes, we predict a maximum rate of $k_{CT} = 2.8 \times 10^5\ s^{-1}$. In any case, the reaction is sufficiently slow to be probed by electron spin resonance (ESR) or time-resolved IR spectroscopy. We have $R = 10.1$ Å as the Ru−C_{60} edge-to-edge distance.

The calculated rates are slow compared to experimental and theoretical values obtained for covalently bonded and stacked π orbital systems such as bridged triarylamines[58,59] and DNA in its double-helical conformation.[43,60] They are, however, as fast as CT between two ruthenium complexes covalently bridged by a oligoglycine linker, which have been computed using the same model as described above.[47] Here, CT rates are smaller than in the Ru−protein−C_{60} system for more than two amino acids separating the two coordinated histidines. As there are no covalent links between the C_{60} fragment and the remainder of the system, CT is purely of the through-space type,[61] in contrast to CT through the protein backbone[47] or alkane chains.[62] Deleting all aromatic side chains that intercalate the donor and the fullerene, we find a donor−acceptor coupling smaller than the numerical resolution achievable ($\sim 10^{-9}$ eV). Consequently,

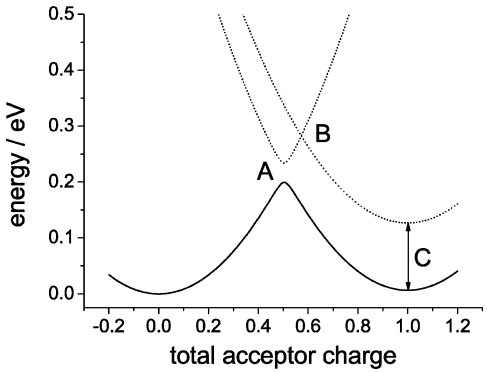

Figure 6. Potential energy as a function of the fullerene charge for a four-orbital model describing charge transfer between a ruthenium d orbital and the three C_{60} LUMOs. Capital letters indicate the low-energy CT path (A), the two high-energy CT paths (B), and the acceptor−acceptor optical transition (C).

these π bridges participate in the CT reaction via a superexchange mechanism.

The curve presented in Figure 4 can be rationalized within a simple four-orbital model, which comprises the donor Ru d orbital and the three fullerene LUMOs as acceptor levels. We introduce a single excess charge $\bar{n}$ and assign an effective electron−electron interaction U to each of the constituents. In the presence of a protein environment, the fullerene LUMO symmetry will be broken, and the new LUMOs will be represented by linear combinations of the old ones, which has a random character due to the fluctuations in C_{60} and its environment. We therefore approximate the excess charge as homogeneously distributed along the three basis functions, i.e., the LUMOs of the isolated fullerene. In the absence of the protein environment, the three C_{60} LUMOs are orthogonal; in its presence, however, we have an effective protein-mediated acceptor−acceptor coupling t_2. Denoting t_1 as the superexchange donor−acceptor coupling, we may write the four-orbital model Hamiltonian matrix as

$$-\mathbf{H} = \begin{pmatrix} 2U(1-\bar{n}) & t_1 & t_1 & t_1 \\ t_1 & 2U\bar{n}/3 & t_2 & t_2 \\ t_1 & t_2 & 2U\bar{n}/3 & t_2 \\ t_1 & t_2 & t_2 & 2U\bar{n}/3 \end{pmatrix} \qquad (7)$$

where again the usual corrections apply for counting the electron−electron interaction twice. We obtain the potential energy curve as a function of $\bar{n}$ as shown in Figure 6. For the sake of convenience, we have considerably exaggerated the donor−acceptor coupling t_1 to 20 meV. Otherwise, the plot is similar to that computed for the entire Ru−antibody−C_{60} system as described above. A more detailed analysis shows that the effective electronic tunnel splitting between the ground state at point A is given by $2t = 2\sqrt{3}t_1$, that the levels crossing at point B do not couple due to their different symmetry, and that the maximum splitting of the acceptor ground state and the two lowest degenerate excited eigenstates equals $3t_2$. For the simulated geometries, these symmetry arguments do not hold any more, and the average couplings are equal for all channels. As the saddle points are approached, additional orbitals mix with the first excited states in the full linear combination of atomic orbitals molecular orbital (LCAO-MO) computation, thus lowering these states as compared to the simple four-orbital model.

In addition to a vertical donor−accptor charge-transfer reaction that can be induced by irradiating light with $E_{opt} = \lambda = 0.86$ eV, we find an acceptor−acceptor absorption at 0.12 eV (as indicated in Figure 6), which corresponds to an infrared excitation at ~970 cm^{-1}, which emerges as a consequence of the splitting of the C_{60} LUMOs in the presence of an excess charge. Of the orbitals participating in the excitation, the ground state exhibits the full symmetry of the fullerene, whereas one of the excited states can be represented by a combination that has the same orientation as a linearly polarized electromagnetic field. Hence, the transition is supposed to be IR-active. We consider this excitation as an additional fingerprint of a CT system involving a fullerene and as a means to verify or falsify our model.

4. Concluding Discussion

We have described CT through a contact between a fullerene and its antibody by an atomistic, chemically specific model. It is based upon an X-ray structure analysis of the antibody's binding site and a molecular dynamics simulation of the complex, to which we have attached a mixed valence ruthenium complex via a hypothetical Tyr52His mutation in the heavy protein chain. The energetics of the CT reaction has been modeled utilizing a Hamiltonian that considers the chemical bond, polarization effects and vibronic contributions. Cross-sections of the potential energy surface have been analyzed to directly obtain the energy parameters relevant to Marcus' theory of CT.

In contrast to simple two-site donor−acceptor models, the LUMO degeneracy of the C_{60} constituent requires a four-orbital model to reproduce the numerical findings. A total of three channels contribute to charge transfer; they are characterized by an equal effective donor−acceptor coupling, but by slightly different activation barriers. As a novel mechanism of protein charge transfer, we find superexchange via aromatic residues that exhibit π-stacking interactions with the fullerene. The resulting reaction rates are comparable to those obtained for protein charge transfer through a short sequence of covalent bonds. The model presented here can be straightforwardly adapted to predict CT rates within more complex bio−nano aggregates including nanotubes, DNA fragments, or conducting polymers.

Acknowledgment. It is a pleasure to acknowledge fruitful discussions with T. Cramer, M. Diez, Th. Friedrich, P. Gräber, A. Labahn, E.B. Starikov, and C.A. Zell. We are particularly indebted to Professor Jianpeng Ma and Dr. William H. Noon (Rice University, Houston) for kindly and generously making their simulation geometries available.

References and Notes

(1) Wilson, L. J.; Cagle, D. W.; Thrash, T. P.; Kennel, S. J.; Mirzadeh, S.; Alford, J. M.; Ehrhardt, G. J. *Coord. Chem. Rev.* **1999**, *192*, 199−207.

(2) Wilson, L. J. *Interface* **1999**, *8*, 24−28.

(3) Dugan, L. L.; Turetsky, D. M.; Du, C.; Lobner, D.; Wheeler, M.; Almli, C. R.; Shen, C. K. F.; Luh, T. Y.; Choi, D. W.; Lin, T. S. *Proc. Natl. Acad. Sci. U.S.A.* **1997**, *94* (17), 9434−9439.

(4) Cagle, D. W.; Kennel, S. J.; Mirzadeh, S.; Alford, J. M.; Wilson, L. J. *Proc. Natl. Acad. Sci. U.S.A.* **1997**, *96* (9), 5182−5187.

(5) Straface, E.; Natalini, B.; Monti, D.; Franceschi, C.; Schettini, G.; Bisaglia, M.; Fumelli, C.; Pincelli, C.; Pellicciari, R.; Malorni, W. *FEBS Lett.* **1999**, *454* (3), 335−340.

(6) Lin, A. M. Y.; Chyi, B. Y.; Wang, S. D.; Yu, H. H.; Kanakamma, P. P.; Luh, T. Y.; Chou, C. K.; Ho, L. T. *J. Neurochem.* **1999**, *72* (4), 1634−1640.

(7) Balavoine, F.; Schultz, P.; Richard, C.; Mallouh, V.; Ebbesen, T. W.; Mioskowski, C. *Angew. Chem., Int. Ed.* **1999**, *38* (13−14), 1912−1915.

(8) Iijima, S. *Nature* **1991**, *354* (6348), 56−58.

(9) Sijbesma, R.; Srdanov, G.; Wudl, F.; Castoro, J. A.; Wilkins, C.; Friedman, S. H.; Decamp, D. L.; Kenyon, G. L. *J. Am. Chem. Soc.* **1993**, *115* (15), 6510−6512.

(10) Braden, B. C.; Goldbaum, F. A.; Bi-Xing Chen, Kirschner, A. N.; Wilson, S. R.; Erlanger, B. F. *Proc. Natl. Acad. Sci. U.S.A.* **2000**, *97*, 12193−12197.

(11) Noon, W. H.; Kong, Y.; Ma, J. *Proc. Natl. Acad. Sci. U.S.A.* **2002**, *99*, 6466−6470.

(12) Noon et al.[11] also report a 200 ps simulation of the antibody molecule submerged in a large periodic water box, leading to a similiar binding pattern as the stochastic boundary method computations used here.

(13) Dittrich, M.; Hayashi, S.; Schulten, K. *Biophys. J.* **2003**, *85*, 2253−2266.

(14) Huo, S.; Wang, J.; Cieplak, P.; Kollman, P. A.; Kuntz, I. D. *J. Med. Chem.* **2002**, *45*, 1412−1419.

(15) Schulte, J.; Bohm, M. C. *Solid State Commun.* **1995**, *93* (3), 249−253.

(16) Winkler, J. R.; Nocera, D. G.; Yocom, K. M.; Bordignon, E.; Gray, H. B. *J. Am. Chem. Soc.* **1982**, *104*, 5798−5800.

(17) Winkler, J. R.; Di Bilio, A.; Farrow, N. A.; Richards, J. H.; Gray, H. B. *Pure Appl. Chem.* **1999**, *71*, 1753−1764.

(18) Marcus, R. A. *J. Chem. Phys.* **1956**, *24*, 966−978.

(19) Marcus, R. A. *J. Chem. Phys.* **1956**, *24*, 979−989.

(20) Marcus, R. A. *Annu. Rev. Phys. Chem.* **1964**, *15*, 155−196.

(21) Hush, N. S. *Trans. Faraday Soc.* **1961**, *57*, 557.

(22) Levich, V. G.; Dogonadze, R. R. *Dokl. Akad. Naui SSSR* **1959**, *124*, 123−126.

(23) Berlin, A. Y.; Kurnikov, I. V.; Beratan, D.; Ratner, M. A.; Burin, A. L. *Top. Curr. Chem.* **2004**, *237*, 1−36.

(24) Wolynes, P. G.; Kuki, A. *Science* **1987**, *236*, 1647−1652.

(25) Kuki, A. *Struct. Bonding* **1991**, *75*, 49−81.

(26) Siddarth, P.; Marcus, R. A. *J. Phys. Chem.* **1993**, *97*, 2400−2405.

(27) Siddarth, P.; Marcus, R. A. *J. Phys. Chem.* **1993**, *97*, 6111−6114.

(28) Siddarth, P.; Marcus, R. A. *J. Phys. Chem.* **1993**, *97*, 13078−13082.

(29) Stuchebrukhov, A. A.; Marcus, R. A. *J. Phys. Chem.* **1995**, *99*, 7581−7590.

(30) Larsson, S. *J. Am. Chem. Soc.* **1981**, *103*, 4034−4040.

(31) Gruschus, J. M.; Kuki, A. *J. Phys. Chem. B.* **1999**, *103*, 11407−11414.

(32) Katz, D. J.; Stuchebrukhov, A. A. *J. Phys. Chem.* **1998**, *109*, 4960−4970.

(33) Lopez-Castillo, J.-M.; Filali-Mouhim, A.; Binh-Otten, E. N. V.; Jay-Gerrin, J.-P. *J. Am. Chem. Soc.* **1997**, *119*, 1978−1980.

(34) Cheung, M. S.; Daizadeh, I.; Stuchebrukhov, A. A.; Heelis, P. F. *Biophys. J.* **1999**, *76*, 1241−1249.

(35) Beratan, D. N.; Betts, J. N.; Onuchic, J. N. *Science* **1991**, *252*, 1285−1288.

(36) Pande, V. S.; Onuchic, J. N. *Phys. Rev. Lett.* **1997**, *78*, 146−149.

(37) Regan, J. J.; Risser, S. M.; Beratan, D. N.; Onuchic, J. N. *J. Phys. Chem.* **1993**, *97*, 13083−13088.

(38) Curry, W. B.; Grabe, M. D.; Kurnikov, I. V.; Skourtis, S. S.; Beratan, D. N.; Regan, J. J.; Aquino, A. J.; Beroza, P.; Onuchic, J. N. *J. Bioenerg. Biomembr.* **1995**, *27*, 285−293.

(39) Beratan, D. N.; Onuchic, J. N.; Winkler, J. R.; Gray, H. B. *Science* **1992**, *258*, 1740−1741.

(40) Onuchic, J. N.; Beratan, D. N.; Winkler, J. R.; Gray, H. B. *J. Biomol. Struct.* **1992**, *21*, 349−377.

(41) Vollmer, E.; Kordel, M.; Koslowski, T. *Z. Phys. Chem.* **2004**, *218*, 611−622.

(42) Koslowski, T. *J. Chem. Phys.* **2000**, *113*, 10703−10711.

(43) Cramer, T.; Krapf, S.; Koslowski, T. *J. Phys. Chem. B* **2004**, *108*, 11812−11819.

(44) Cramer, T.; Volta, A.; Blumen, A.; Koslowski. T. *J. Phys. Chem. B* **2004**, *108*, 16586−.

(45) Cramer, T.; Krapf, S.; Koslowski, T. *Phys. Chem. Chem. Phys.* **2004**, *6*, 3160−.

(46) Cramer, T.; Steinbrecher, T.; Labahn, A.; Koslowski, T. *Phys. Chem. Chem. Phys.* **2005**, *7*, 4039−.

(47) Utz, N.; Engel, L.; Friedrich, T.; Koslowski, T. *Z. Phys. Chem.* **2005**, *219*, 1391−.

(48) Frisch, M. J.; Trucks, G. W.; Schlegel, H. B.; Scuseria, G. E.; Robb, M. A.; Cheeseman, J. R.; Montgomery, J. A., Jr.; Vreven, T.; Kudin, K. N.; Burant, J. C.; Millam, J. M.; Iyengar, S. S.; Tomasi, J.; Barone, V.; Mennucci, B.; Cossi, M.; Scalmani, G.; Rega, N.; Petersson, G. A.; Nakatsuji, H.; Hada, M.; Ehara, M.; Toyota, K.; Fukuda, R.; Hasegawa, J.; Ishida, M.; Nakajima, T.; Honda, Y.; Kitao, O.; Nakai, H.; Klene, M.; Li, X.; Knox, J. E.; Hratchian, H. P.; Cross, J. B.; Bakken, V.; Adamo, C.; Jaramillo, J.; Gomperts, R.; Stratmann, R. E.; Yazyev, O.; Austin, A. J.; Cammi, R.; Pomelli, C.; Ochterski, J. W.; Ayala, P. Y.; Morokuma, K.; Voth, G. A.; Salvador, P.; Dannenberg, J. J.; Zakrzewski, V. G.; Dapprich, S.; Daniels, A. D.; Strain, M. C.; Farkas, O.; Malick, D. K.; Rabuck, A. D.; Raghavachari, K.; Foresman, J. B.; Ortiz, J. V.; Cui, Q.; Baboul, A. G.; Clifford, S.; Cioslowski, J.; Stefanov, B. B.; Liu, G.; Liashenko, A.; Piskorz, P.; Komaromi, I.; Martin, R. L.; Fox, D. J.; Keith, T.; Al-Laham, M. A.; Peng, C. Y.; Nanayakkara, A.; Challacombe, M.; Gill, P. M. W.; Johnson, B.; Chen, W.; Wong, M. W.; Gonzalez, C.; Pople, J. A. *Gaussian 03*, revision B.04; Gaussian, Inc.: Pittsburgh, PA, 2003.

(49) Harrison, W. A. *Electronic Structure and the Properties of Solids*; Freeman: San Francisco, 1980.

(50) Slater, J. C.; Koster, G. F. *Phys. Rev.* **1954**, *94*, 1498.

(51) Su, W. P.; Schrieffer, J. R.; Heeger, A. J. J. *Phys. Rev. Lett.* **1979**, *42*, 1698.

(52) Rateitzak, M.; Koslowski, T. *Chem. Phys. Lett.* **2003**, *377*, 455−461.

(53) Micnas, R.; Ranninger, J.; Robaszkiewicz, S. *Rev. Mod. Phys.* **1990**, *62*, 113−171.

(54) Marinaro, M.; Matsumoto, H.; Mancini, F. *Int. J. Mod. Phys. B* **1996**, *10*, 1717−1734.

(55) Rauhut, G.; Clark, T. *J. Am. Chem. Soc.* **1993**, *115*, 9127−9135.

(56) Warshel, A. *Acc. Chem. Res.* **2002**, *35*, 385−395.

(57) Bader, J. S.; Chandler, D. *Chem. Phys. Lett.* **1989**, *157*, 501−504.

(58) Lambert, C.; Nöll, G. *J. Am. Chem. Soc.* **1999**, *121*, 8434.

(59) Utz, N.; Koslowski, T. *Chem. Phys.* **2002**, *282*, 389−397.

(60) Hall, D. B.; Holmlin, R. E.; Barton, J. K. *Nature* **1996**, *382*, 731−735.

(61) Page, C. C.; Moser, C. C.; Dutton, P. L. *Curr. Opin. Chem. Biol.* **2003**, *7*, 551−556.

(62) Cukier, E.; Cave, R. J. *Chem. Phys. Lett.* **2005**, *402*, 186−191.